GM2 ganglioside accumulation causes neuroinflammation and behavioral alterations in a mouse model of early-onset Tay-Sachs disease.

Secil Akyildiz Demir
Izmir Yuksek Teknoloji Enstitusu
Zehra Kevser Timur
Izmir Yuksek Teknoloji Enstitusu
Nurselin Ates
Izmir Yuksek Teknoloji Enstitusu
Luis Alarcon Martinez
Hacettepe Universitesi Tip Fakultesi
Volkan Seyrantepe (volkanseyrantepe@iyte.edu.tr)
Izmir Yuksek Teknoloji Enstitusu https://orcid.org/0000-0002-0243-5011

Research

Keywords: Tay-Sachs disease, GM2, mouse model, neuroinflammation, behavior

Posted Date: January 8th, 2020

DOI: https://doi.org/10.21203/rs.2.20299/v1

Version of Record: A version of this preprint was published on September 20th, 2020. See the published version at https://doi.org/10.1186/s12974-020-01947-6.

Abstract

Background

Tay-Sachs disease (TSD), a type of GM2-gangliosidosis, is a progressive neurodegenerative lysosomal storage disorder, caused by mutations in the a subunit of lysosomal β-hexosaminidase enzyme. This disease is characterized by excessive accumulation of GM2 ganglioside, predominantly in the central nervous system. Although Tay-Sachs patients appear normal at birth, the progressive accumulation of undegraded GM2 gangliosides in neurons leads to death. Recently, an early-onset Tay-Sachs disease mouse model with genotype Hexa-/-Neu3-/- was generated. Progressive accumulation of GM2 led to premature death of the double KO mice. Importantly, this double-deficient mouse model displays typical features of Tay-Sachs patients, such as cytoplasmic vacuolization of nerve cells, deterioration of Purkinje cells, neuronal death, deceleration in movement, ataxia and, tremors. GM2-gangliosidosis is characterized by acute neurodegeneration preceded by activated microglia expansion, macrophage and astrocyte activation, along with the production of inflammatory mediators. However, the mechanism of disease progression in Hexa-/-Neu3-/- mice relevant to neuroinflammation is poorly understood.

Method

We investigated the onset and progression of neuropathological and neuroinflammatory changes in the cortex, cerebellum and retina of Hexa-/-Neu3-/- mice and littermate wild-type as well as Hexa-/- and Neu3-/- mice by using a combination of expression, immunofluorescence and behavioral analyses.

Results

We found elevated levels of pro-inflamatory pro-inflammatory cytokine and chemokine transcripts, such as Ccl2, Ccl3, Ccl4 and Cxcl10 and also extensive microglial and astrocyte activation and proliferation accompanied by in peripheral blood mononuclear cell infiltration in neurons and oligodendrocytes. Behavioral tests demonstrated high level of anxiety, and age dependent loss in both memory and muscle strength in Hexa-/-Neu3-/- mice compared with that in the controls.

Conclusion

Altogether, our data suggest that Hexa-/-Neu3-/- mice display a phenotype similar to human TSD patients suffering from chronic neuroinflammation triggered by GM2 accumulation. Our observations collectively suggest a hypothesis that modulation of Ccl2, Ccl3, Ccl4 and Cxcl10 or of their receptors, in combination with traditional drugs such as propagermanium, may provide a novel approach for the management of disease and better understanding of the neuropathology in a mouse model of early-onset Tay-Sachs disease.

Background

Tay-Sachs disease (TSD) is a fatal inherited lysosomal storage disorder, principally affecting the brain, which leads to neurological dysfunction. TSD is cuased by mutations in the Hexa gene which encodes the α-subunit of lysosomal β-hexosaminidase α (HEXA), an enzyme that converts GM2 to GM3 ganglioside [1, 2]. Infants with TSD appear healthy at birth but progressive GM2 accumulation causes loss of motor function and cognition, developmental regression, dystonia, blindness, seizures and death in childhood [1].

Unlike in TSD patients, the phenotype of Hexa-/- knockout (KO) mice was nearly normal with limited ganglioside storage in the nervous system [1–3]. This result was due to a metabolic bypass in Hexa-/- mice, specifically in the NEU3 sialidase-mediated hydrolysis of sialic acid from stored GM2, yielding GA2 ganglioside, which is further degraded by the functional HEXB [3, 4].

Early-onset Tay-Sachs disease mouse model (Hexa-/-Neu3-/-) was generated by crossing of Hexa-/- and Neu3-/- mice to investigate the role of NEU3 sialidase in GM2 ganglioside degradation [5]. These mice were healthy at birth, but died at 1.5 to 4.5 months of age, equivalent to the life expectancy of Tay-Sachs patients. It has been shown that abnormal accumulation of GM2 ganglioside in neurons leads to cytoplasmic vacuolation and progressive neurodegeneration, resulting in neuronal death, Purkinje cell depletion, and astrogliosis. Hexa-/-Neu3-/- mice also exhibited neurobehavioral abnormalities such as growth delay, abnormalities in the skeletal bones, slow movement, ataxia, and tremors. Consequently, the Hexa-/-Neu3-/- mouse model mimics the pathological, biochemical and clinical abnormalities of the Tay-Sachs patients, and is particularly useful to further understand the pathologies and cellular and molecular mechanisms underlying the progression of TSD [5].

A previous study showed that storage of GM1 and GM2 gangliosides in the CNS led to microgliosis and astrogliosis, and that the degree of inflammation is correlated with increased levels of ganglioside accumulation. While inflammation markers including inflammatory cytokines (TNFα, IL1β and TGFβ1) were absent in Hexa$^{-/-}$ mice, they were significantly expressed in the Hexb-/- mouse model of Sandhoff disease (SD). GM1 gangliosidosis mouse model [6], and GM2-gangliosidosis patients [7]. Activation of microglia and astrocytes resulted in the production of inflammatory mediators [8]. For instance, the levels of TNF-α pro-inflammatory cytokine were significantly increased in the cerebrospinal fluid of TSD patients [9]. In addition, five inflammation biomarkers, ENA-78, MCP-1, MIP-1α, MIP-1β, and TNFR2 were also detected in the cerebrospinal fluid of patients with infantile and juvenile gangliosidosis [10]. Various lysosomal storage disorders including Niemann–Pick type C disease [11], Gaucher disease [12], mucopolysaccharidosis type I, IIIA and III [13] and neuronal ceroid-lipofuscinoses [14] also exhibit neuropathological alterations such as, prominent microglial and astrocyte activation. A previous study showed that Hexa-/-Neu3-/- mice exhibited an inflammatory response, with astrogliosis in the hippocampus, cortex and cerebellum [5]. In this work, we aimed to further investigate the neuroinflammatory response to GM2 accumulation in the brain and retina of Hexa-/-Neu3-/- mice, and its effect on behavior during the progression of disease.

Methods

Animals

Hexa-/- on a 129/Sv background [3] and Neu3-/- on a C57BL/6 background [15] were bred in a laboratory animal facility, at the Izmir Institute of Technology to generate mice of the target genotype; WT, Hexa-/-, Neu3-/- and Hexa-/-Neu3-/-. Breeding and genotyping of these mice was performed as previously described [5]. Genotypes were determined from tail samples using standard PCR procedures and the following primers: Hexa primers; HexaF (5"-GGCCAGATACAATCATACAG-3"), HexaR (5"-CTGTCCACATACTCTCCCCACAT-3") and PGKR (5"-CACCAAAGAAGGGAGCCGGT-3") and Neu3 primers Neu3F (5"-AAGCAGAGAACATTCTTGAGAGAGCACAGC-3"), Neu3R (5"-TCGTGCTTTACGGTATCGCCGCTCCCGATT-3"), and NeoR (5"-GTGAGTTCAAGAGCCATG TTGCTGATGGTG-3"). The mice were maintained at a constant temperature with an alternating 12-h light/dark cycle. Food and water were available ad libitum. The protocols used to perform the experiments described in this work were approved by the Institutional Animal Care and Use Committee of the İzmir Institute of Technology.

RNA array for cytokine and chemokine-encoding genes

For a broad analysis of inflammatory gene expression in the cortex and cerebellum of Hexa-/- and Hexa-/-Neu3-/- mice, the mRNA profile of cellular mediators of inflammation, specifically cytokine and chemokines was assessed using RT² Profiler PCR Array (Qiagen, The Netherlands) according to manufacturer's instructions. Total RNA was transcribed using the RT^2 First Strand Kit (Qiagen, The Netherlands). Real-Time SYBR green PCR master mix (Qiagen, The Netherlands) was used and PCR cycles were programmed in accordance with the manual. Briefly, (10 min at 95 °C, followed by 40 cycles of 15 s at 95 °C for and 1 min at 60 °C) followed by routine melting curve analysis. All data were normalized to an average of five housekeeping genes, i.e. Gusb, Hprt, Hsp90ab1, GADPH and Actb . Each sample had a single peak in each reaction at a temperature greater than 80°C which showed that there is no non-specific product. The threshold cycle changes ($\triangle$Ct) denote the difference in Ct for the gene of interest based on the Ct level of housekeeping genes. Expression of each gene was normalized using the mean expression of five different housekeeping genes in the array. Fold changes in the expression level of genes were obtained according to the $2^{-\Delta\Delta CT}$ method. Significant differences between genotypes were analyzed by Student's t-test. Genes that had positive or negative fold changes of more than 1.5 fold with a p-value smaller than 0.05, were considered to be statistically significant.

Immunofluorescence analysis

Mice were deeply anesthetized (Ketamine/xylazine; 200/10 mg/kg) and perfused with fixative (4% paraformaldehyde in PBS, pH7.4). Brains were removed and post-fixed in the same fixative solution, overnight at 4°C; and then sequentially treated with 10%, 20%, and 30% sucrose in PBS. Brains were embedded in Tissue-Tek OCT compound (Sakura Finetechnical, Tokyo, Japan), and frozen at -80 ^{0}C. Frozen brain specimens were sectioned at 10 µm thickness, and mounted on HistoBond®microscope slides (Marienfeld, Germany) at −20°C, using a Leica cryostat. Coronal brain slices (10 µm) obtained from

the mice at the indicated ages were treated with ice-cold acetone, and then, blocked using blocking buffer (4% BSA, 10% goat serum, 0.3% Triton X-100 and 0.3 M glycine in PBS), for 1 h at room temperature in a humidified chamber. Anti-GM2 (GM2 ganglioside;1:500; KM966), anti-CD45 (1:300; Santa Cruz Biotechnology, U.S.A.), anti-Moma2 (1:50; Abcam, USA), anti-LAMP1 (1:500; Abcam, USA), anti-CNPase (1:50; Cell Signaling Technology, The Netherlands) and anti-NeuN (1:100; Cell Signaling Technology, The Netherlands) were diluted in blocking buffer and applied overnight at 4 °C. The following Alexa Flour conjugated secondary antibodies was used to visualize target primary antibodies; goat anti-rabbit Alexa Fluor 568 (Abcam, USA), goat anti-rabbit Alexa Fluor 488 (Abcam, USA), goat anti-rat Alexa Fluor 568 (Abcam, USA). anti-IL6 (1:250; Santa Cruz Biotechnology, U.S.A.) antibody was diluted in the blocking buffer (4% BSA, 10% goat serum, 0.3% Triton X-100 and 0.3 M glycine in PBS) overnight and it was labelled with donkey anti-goat Alexa Fluor 555 (Abcam, USA). The slides were mounted with Fluoroshield mounting medium with DAPI (Abcam, USA) and images were obtained using light microscope (Bx53, Olympus Corporation, Germany) equipped with a manually controlled specimen; a color camera (DP73, Olympus Corporation, Germany); a fluorescent light source (U-RFL-T, Olympus Corporation, Germany); and an image analysis software (cellSens Entry, Olympus Corporation, Germany).

Retina analysis

Eyes were removed and fixed for 24 hours with 4% PFA, at room temperature. Retinas were prepared as flattened whole-mounts, by making four radial cuts, and labelled with anti-lectin (20µg/mL) (Vector Laboratories, USA) and anti-phalloidin (1:100)(Biotium, USA). Retinas were permeabilized by washing in PBST for 30 min, then, washed them in PBS 3 times for 10 min and, finally, anti-lectin was applied at 4^{o}C overnight. The following day, they were washed in PBS 3 times for 5 min and incubated in anti-phalloidin at 4 ^{o}C overnight. Retinas were mounted with anti-fade reagent containing Hoechst-33258 to label nuclei (Molecular Probes, USA). Twenty µm-thick sagittal sections were assessed for potential anatomical alterations. Finally, whole-mount retinas and sagittal sections were imaged using light microscope (400x, Eclipse E600, Nikon Instruments Inc., Japan) equipped with a manually controlled specimen stage for X, Y, and Z-axis; a color camera (model DXM1200, Nikon Instruments Inc., Japan); a fluorescent light source (HB-10104AF, Nikon Instruments Inc., Japan); and an image analysis software (NIS-Elements, Version 3.22, Nikon Instruments Inc., Japan).

Passive avoidance test

This test was conducted as previously described [16] . The apparatus is divided into a lit compartment and a dark compartment with a vertical sliding door between the two. Briefly, each mouse was placed into the bright compartment, and after 30 s the central door opened allowing it to migrate into the dark compartment, which they generally prefer. The following day, upon entry into the dark compartment, the door was closed and the mouse received a mild electric shock (0.2 mA for 2 s). On the final day, animals were given the same choice to enter the dark compartment (300 s maximum time). Latency time for to cross through the door between compartments was scored with ShutAvoid v1.8 (Harvard Apparatus, USA).

Morris water maze test

Spatial memory and memory were assessed as previously described [16]. The water maze consists of a large circular pool (diameter 140 cm; depth, 45 cm) filled with an opaque solution of dry milk in water (22 ^{0}C), that is located in a room with numerous visual cues. Spatial acquisition was organized in 3 training sessions (days 1-3) with a visible platform (1 cm above the platform). Each mouse has 60 s to reach the platform. The location of cues and platform were changed every day and the mice were released into the water at 3 different locations. On days 4-8 animals received reversal training with an invisible platform (1 cm below the water surface). For this training the platform location was kept constant, and mice were placed into the water at 3 different locations and given 90 s to find the platform. Measurements were acquired with a Sony camera (model SSC-G18), centrally positioned above the water tank. Behavioral differences were analyzed using the Panlab SMART Video Tracking System v0.3 (Harvard Apparatus, USA). Animals were allowed to dry under heat lamp after each trial to avoid hypothermia, and all experiments were started at the same time each day.

Grip strength

Mice were subjected to forelimb grip strength test, with a Grip Strength Meter (IITC Life Science, USA). The gauge was reset to 0 g after stabilization, and each mouse was encouraged to grab a T-shaped bar. Connection of the bar to a digital force transducer allowed quantification of strength as pull force in grams. The order of mice tested was randomized, and the inspector was blinded to genotypes of mice.

Open field test

The apparatus for this assay, consisted of a 40x40 cm in surface area, and was surrounded from all sides by a 40 cm transparent wall. A digital camera was mounted directly above the apparatus. Mice were placed in one of the corners of the open field, and allowed to explore undisturbed for 5 min. Behavioral differences were analyzed using the Panlab SMART Video Tracking System v0.3 (Harvard Apparatus, USA).

Statistical analysis

GraphPad QuickCalcs (GraphPad Software, USA) software was used for the statistical analysis. All values are expressed as the mean ± S.E.M. Differences were tested using one-way-ANOVA for behavioral analysis and immunofluorescence analysis. qPCR data were analyzed by unpaired *t*-test. A p-value of less than 0.05 was considered to represent statistical significance.

Results

Altered level of GM2 ganglioside

A previous study showed significantly higher levels of GM2 ganglioside accumulation in the brain of 4.5-month-old Hexa-/-Neu3-/- mice compared to Hexa-/- using HPTLC and mass spectrometric analysis [5]. In

this study, 10 µm coronal brain sections from 4.5-month-old WT, Hexa-/-, Neu3-/- and double-deficient Hexa-/-Neu3-/- mice were immunostained with anti-GM2 antibody. As shown in Supp. Fig. 1, the number of neuron cells with GM2 accumulation was significantly increased in CA1, CA2, and CA3 hippocampal regions (7-fold), primary motor and somatosensory area of the cerebral cortex (7-fold), thalamus (7.5-fold), Purkinje and granular layers of the cerebellum (18-fold) and pons (7.5-fold) of Hexa-/-Neu3-/- mice compared with that in Hexa-/- mice. GM2 ganglioside accumulation was also observed in the retrosplenial cortex and secondary motor cortex (data not shown). No GM2 was detected in WT and Neu3-/- mice.

Altered levels of the inflammatory cytokines and chemokines

The presence of neuroinflammatory conditions such as astrogliosis in the hippocampus, cortex and cerebellum of 4.5-month-old Hexa-/-Neu3-/- mice has been previously shown [5]. In this study we found that activated astrocytes are present in the hippocampus, cortex and cerebellum of both 2.5- and 4.5-month-old Hexa-/-Neu3-/- mice (Supp. Fig. 2). Neuroinflammation involves the release of inflammatory cytokines and chemokines [17]. Therefore, we evaluated the levels of pro- and anti-inflammatory cytokines and chemokines in the cortex and cerebellum of 4.5- month-old Hexa-/- and Hexa-/-Neu3-/- mice. We used a preformatted gene pathway array to compare the expression of 84 inflammatory chemokine, cytokine and interleukin receptor genes relative to that in Hexa-/- mice. After disregarding unregulated, non-detectable gene products and evaluating the relative levels of gene expression across all samples, we identified 42 inflammatory genes, which we categorized into 3 distinct groups.

Pro-inflammatory cytokines and chemokines, secreted mostly by activated macrophages in microglial cells, are involved in the up-regulation of inflammatory reactions (Zhang and An 2007). Our data showed that Hexa-/-Neu3-/- mice compared to Hexa-/- mice displayed an altered expression profile for pro- and anti-inflammatory cytokines and chemokines in both cortex (Fig. 1A) and cerebellum (Fig. 1B) regions. Major increases were seen in Ccl2 (11.3-fold), Ccl3 (12-fold), Ccl4 (24.4-fold), and Cxcl10 (17.2-fold) in cortex of mice (Fig. 1A). Ccl3 (17.2 fold), Ccl4 (41 fold), and Cxcl13 (5 fold) were predominantly expressed in the cerebellum. It has been established that Ccl2 cytokine displays chemotactic activity for monocytes, lymphocytes and neutrophils while Ccl3 is involved in the migration of monocytes, lymphocytes, and neutrophils together with Ccl2 [19] and activates T cells and macrophages with Ccl4 [20]. Increased expression of Ccl3 and Ccl4 in brain and cerebellum were also shown in different lysosomal storage diseases such as MPSIIIA [21] and MPSIIIB [22] and Gaucher Disease [23, 24]. In addition, Cxcl10, an inflammatory chemokine produced by astrocytes which, recruits activated T lymphocytes by increasing their migration to the site of tissue damage, is increased in both cortex and cerebellum of Hexa-/-Neu3-/- [25, 26]

Anti-inflammatory cytokines and chemokines regulate the expression of pro-inflammatory cytokines to arrest or slow down the immune response [18]. We found not only up-regulation of pro-inflammatory cytokines and chemokines in Hexa-/-Neu3-/- mice (Fig.1A, B); but also down-regulation of anti-inflammatory cytokines and chemokines which provides a more complete pictures of the inflammatory

conditions in the cortex (Fig.1C) and cerebellum (Fig. 1D). Analysis of anti-inflammatory cytokines and chemokines revealed a significant decrease in the levels of IL10 (2.6-fold), IL11 (3.6-fold), IL13 (3.2-fold), IL2 (3.1-fold), IL22 (2.9-fold) and IL4 (3.2-fold) in the cortex of double deficient Hexa-/-Neu3-/- mice compared to Hexa-/-. In addition, we found that, IL10 (1.2-fold), IL11 (1.3-fold), IL13 (7.8- fold), IL2 (5.3-fold) and IL24 (5-fold) were significantly decreased in the cerebellum of Hexa-/-Neu3-/- mice, compared to Hexa-/-. IL10 protect tissues by preventing excessive inflammation to [27], and IL13 has a similar immunosuppressant activity [28]. Decreased expression of IL10 and IL13 in cortex and cerebellum was thought to contribute to the neuroinflammation seen in Hexa-/-Neu3-/- mice.

Expression levels of growth factors in cortex (Fig. 1E) and cerebellum (Fig. 1F) of Hexa-/-Neu3-/- mice were also analyzed. We found that the expression ratio of Bmp2 (1.2- fold), Bmp4 (2.3-fold), Bmp6 (2.5-fold), Bmp7 (1.7-fold), Csf3 (7.1-fold) in the cortex was lower than Hexa-/- mice, whereas the expression ratio of Csf1 (1.6-fold) and Lif (3.4-fold) was higher. In the cerebellum, Bmp2 (2.2-fold), Bmp4 (1.1-fold), Bmp6 (1.3-fold), Csf3 (2.2-fold) were decreased while Csf1 (1.3 fold) was increased compared with that in Hexa-/- mice. Csf1, a cytokine that controls the production, differentiation, and function of macrophages [29], was increased in cortex (1.6-fold) and cerebellum (1.3-fold) of Hexa-/-Neu3-/- mice, which may account for the higher number of macrophages seen in these regions (Fig. 1H, P). The Bmp protein family is responsible for the regulation of bone formation, maintenance and repair [30]. Decreased expression of Bmp2, 4, 6, and 7 may be a contributing factor to the hunched posture observed in Hexa-/-Neu3-/- mice [5]. Increased level of Lif under inflammatory conditions has been shown to inhibit cell proliferation [31], a similar increase was observed in the cortex of Hexa-/-Neu3-/- mice. Csf3 is responsible for the production and differentiation of granulocytes and is involved in defense against pathogens. Decreased inexpression of Csf3 might result in predisposition of Hexa-/-Neu3-/- mice to bacterial infection

Microglial activation

Microglial cells are the immune cells of the CNS responsible for sensing stress signals released from damaged or dying neurons [20]. They migrate to sites of injury where they release cytokines to promote removal of dead and dying cells by phagocytosis [32]. Once activated, they can act to activate neighboring microglia, astrocytes, neurons, or oligodendrocytes. Lysosomal storage disorders, including gangliosidosis, result in activation of neuroinflammatory response in the CNS [20]. Under normal conditions microglial cells remain inactive, however the accumulation of undegraded macromolecules activates these cells, causing an increased inflammatory response [17]. Here, we found that the accumulation of GM2 in the cortex and cerebellum led to microglial activation and consequent production of pro-inflammatory cytokines (Fig. 1A, B). To visualize the location of active microglia in Hexa-/-Neu3-/- mice, brain sections from WT, Hexa-/-, Neu3-/- and Hexa-/-Neu3-/- mice were immunostained with the anti-Moma2 and anti-Lamp1 antibodies, which are specific to the activated microglial/macrophage system [33]. The number of Moma2-positive cells was significantly increased in the hippocampus, cortex, thalamus, cerebellum and pons of Hexa-/-Neu3-/- compared with that in WT,

Hexa-/- and Neu3-/- mice at both mice at 2.5 and 4.5-months of age (Supp. Fig. 3 and Fig. 2, respectively).

Microglial activation was statistically analyzed using Image J software. We found significantly increased microgliosis in the brains of 4.5-month-old Hexa-/-Neu3-/- mice compared with that in age-matched Hexa-/- mice, with the following ratios: approximately 60-fold in hippocampus (Fig. 2V), 9-fold in cortex (Fig. 2W), 13-fold in thalamus (Fig. 2X), 19-fold in pons (Fig. 2Z). In the cerebellum, microgliosis was observed only in Hexa-/-Neu3-/- mice (Fig. 2P, Y). Significantly increased amount of microgliosis was also observed at 2.5 months of age Hexa-/-Neu3-/- brain compared to age-matched Hexa-/-Neu3-/- mice as approximately 37 fold in hippocampus (Supp. Fig. 3V), 4 fold in the cortex (Supp. Fig. 3W), and 5 fold in the thalamus (Supp. Fig. 3X). In cerebellum (Supp. Fig. 3P, Y) and pons regions microgliosis was observed only in Hexa-/-Neu3-/- mice (Fig. 2U, Z). There was no microglial activation in the hippocampus, cortex, thalamus and cerebellum of WT and Neu3-/- mice, with the exception of in the pons area.

Increased IL-6 expression in the neuron

Elevated IL6 (proinflammatory cytokine), production due to activated microglia was observed in lysosomal storage disorders, e.g, in the brains of Gaucher disease mouse model, in the serum of Gaucher, Fabry and mucopolysaccharidosis type IVA patients [20, 34–36]. To detect neuronal expression of IL6, brain sections 4.5-month-old WT, Hexa-/-, Neu3-/- and Hexa-/-Neu3-/- mice were immunostained with anti-IL6 antibody.

The number of IL6-positive cells was significantly increased in the hippocampus, cortex, thalamus, and pons of Hexa-/-Neu3-/- compared with that in WT, Hexa-/- and Neu3-/- (Supp. Fig. 4). There was no significant change in number of IL6-positive cells in the cerebellum of WT, Hexa-/-, Neu3-/- and Hexa-/-Neu3-/- mice (Supp. Fig. 4). We found, approximately 3-fold increase in IL6-positive cells in the hippocampus (Supp. Fig. 4V), cortex (Supp. Fig. 4W) and thalamus (Supp. Fig. 4X) of Hexa-/-Neu3-/- mice compared with that in age-matched Hexa-/- mice.

Increased infiltration of peripheral blood mononuclear cells (PBMCs) in the brain

Neuroinflammation contributes to disease progression in several brain disorders. Specifically, activated immune cells induce the infiltration of T and B cells into the CNS, promoting the release of chemokines and stimulating the migration of more immune cells to the CNS via a disrupted BBB [37]. Previous studies showed that neuroinflammation leads to significant infiltration of PBMC in the brain of the Sandhoff mouse model [38]. PBMCs consist of lymphocytes (T cells, B cells, and NK cells), monocytes, and dendritic cells [39].

The PCR Array analysis revealed that transcription levels of Ccl2, Ccl3, and Cxcl10 were significant infiltration in both cortex and cerebellum of Hexa-/-Neu3-/- mice compared with that in Hexa-/- mice (Fig. 2A, B, respectively). Ccl2, Ccl3 and Cxcl10 play various roles in the attraction, migration, and activation of monocytes, lymphocytes, and neutrophils in the CNS. To analyze the presence of activated PBMC in

Hexa-/-Neu3-/- mice, 10µm coronal brain sections from 4.5-month-old WT, Hexa-/-, Neu3-/- and Hexa-/-Neu3-/- were immunostained with anti-CD45 antibody. The average number of CD45-positive cells in the hippocampus, cortex, and thalamus of Hexa-/-Neu3-/- mice was significantly increased compared with that in WT, Hexa-/- and Neu3-/- (Fig. 3). Similarly, activated PBMC were significantly increased in the cerebellum (2.5-fold) of Hexa-/-Neu3-/- mice (Fig. 3P) compared with that in Neu3-/- mice (Fig. 3Y) as well as in the pons (3-fold) of Hexa-/-Neu3-/- mice (Fig. 3U) compared with that in WT mice (Fig. 3Z). Readily detectable numbers of CD45-positive cells were also identified in the cerebellum and pons of WT (Fig. 3M, R, respectively) Hexa-/- (Fig. 3N, S, respectively) and Neu3-/- (Fig. 3O, T, respectively). Thus, progression of TSD could be associated with disruption of the BBB, and widespread infiltration of inflammatory immune cells into the CNS.

Decrease number of oligodendrocyte and neurons

To characterize the degree to which neuroinflamation affected neuron cells and oligodendrocytes, 10 µm coronal brain sections from 2.5 and 4.5-month-old WT, Hexa-/-, Neu3-/- and Hexa-/-Neu3-/- mice were immunostained with NeuN and CNPase antibodies, which recognize nonspecific neurons and oligodendrocytes, respectively. As shown in Fig. 4, 4.5-month-old mice showed loss in neuronal density compared to age-matched control groups, in different regions of the central nervous system. It was demonstrated that the number of NeuN-positive neurons was significantly reduced by approximately 50% in cortex, by approximately 40% in thalamus and by approximetly 50% in pons of Hexa-/-Neu3-/- mice (Fig. 4D, H, P, respectively) compared with that in WT mice (Fig. 4A, E, M, respectively). There was no significant change neuronal density, in the granular layer of the cerebellum (Fig. 4T). Furthermore, there was no significant change in the number of neuron in 2.5-month-old mice compared with that in age-matched control groups in different regions of the central nervous system (Supp. Fig. 5). Loss of NeuN immunoreactivity could be explained by neuronal death in damaged areas of the brain [40]. Thus, a decrease in NeuN immunostaining correlates with increased numbers of apoptotic cells. In previous study, TUNEL assay showed that there was apoptotic cell death in the brain of Hexa-/-Neu3-/- mice compared with that in WT, Hexa-/- and Neu3-/- mice [5]. Furthermore, NeuN-positive neurons in the cortex (Fig. 4D), thalamus (Fig. 4*H*), and hippocampus (Fig. 4P) appeared swollen, with accumulated storage material as previously shown in the Sandhoff mice brain [41].

Oligodendrocytes are, types of glial cells, that function in the formation of myelin which then provides support and insulation to axons [32]. Oligodendrocytes provide axons with myelin sheaths, and have the ability to renew their myelin sheaths three times within a day. Myelination is essential for optimal signal transduction in the CNS. Activated microglia produces various pro-inflammatory mediators, chemokines and cytokines. In such environments, oligodendrocytes are particularly susceptible to microglia-derived factors, resulting in the production of poor-quality myelin sheaths and oligodendrocyte death [42]. As shown in Fig.5 Hexa-/-Neu3-/- mice showed lower numbers of 2',3'-cyclic-nucleotide 3'-phosphodiesterase-positive cells compared with age-matched WT, Hexa-/- and Neu3-/- mice. The number

of oligodendrocytes was reduced by approximately 45% in the cortex, by approximately 55% in thalamus and cerebellum and by approximately 35% in pons area of Hexa-/-Neu3-/- mice (Fig. 5D, H, L, P, respectively) compared with that in WT mice (Fig. 5A, E, I, M, respectively). The number of oligodendrocytes was significantly decreased in the cortex of Hexa-/- mice by approximately 30% compared with that in WT mice. We observed no significant changes in the number of oligodendrocytes in the thalamus, cerebellum and pons of Hexa-/- (Fig. 5F, J, N, respectively) and Neu3-/- (Fig. 5G, K, O, respectively) mice, compared with that in WT mice. These results are consistent with previous studies. Gene expression profile studies in cerebral cortex of normal and GM2 gangliosidosis (Tay-Sachs and Sandhoff) patients revealed that, the myelin basic protein gene, expressed by oligodendrocytes, was also significantly depressed [8]. Sialiated gangliosides, especially GD1a and GT1b, are present on the axonal membrane, and interact with the MAG on the periaxonal surface of to promote myelin sheath stability [43]. GM2 is also a sialic acid containing ganglioside; thus accumulation of GM2 could lead to instability of myelin sheath. We found no significant changes in the number of oligodendrocytes in 2.5-month-old Hexa-/-Neu3-/- mice compared with that in age-matched control groups (Supp. Fig. 6).

Increased number of microglial reaction in the retina

Neuroinflammation or neurodegeneration lead to reactive gliosis in the retina through hypertrophy, causing a thickening and enlargement of processes via Müller cells and astrocytes [44]. To characterize neuroinflammatory conditions affected the retinas, coronal eye sections from 4.5-month-old WT and Hexa-/-Neu3-/- mice at were immunostained with anti-lectin (vessels and glia) and anti-phalloidin antibody (vessels and actin filaments). We found significantly higher numbers of microglia cells in the retinas of Hexa-/-Neu3-/-, mice compared with that in WT mice (Fig. 7A, D). Microglial staining was prominent around the vessels. However, sagittal sections of Hexa-/-Neu3-/- mice showed no anatomical alterations in their retinal layers (Fig. 7G).

Impairments in spatial learning and memory

Up-regulation of cytokines and their receptors within the CNS during inflammation and concomitant effects on brain function have been reported [6]. Morris water maze task was used to detect spatial learning and memory deficits [45–48]. We used a two-way ANOVAS t0 analyze the date. Here we report that both 2.5 and 4.5-month-old Hexa-/-Neu3-/- mice displayed deficits in spatial learning and memory. Also, we found that WT ($p<0.001$), Hexa-/- ($p<0.025$) and Neu3-/- ($p<0.05$) mice learned to use the visual clues to quickly reach the visible platform in the first 3 days of training, whereas Hexa-/-Neu3-/- mice took a longer time to swim toward the platform (Fig. 7A, C). All groups initially had difficulty in finding the exact location of the hidden platform on day 4. While WT, Hexa-/- and Neu3-/- mice groups quickly improved their ability to find the platform, both ($p<0.01$) 2.5 and ($p<0.025$) 4.5-month-old Hexa-/-Neu3-/- mice were not able to learn the location of the hidden platform compared to WT. Also, 2.5-month-old WT ($p<0.025$), Hexa-/- ($p<0.05$) and Neu3-/- (p=ns) mice and 4.5-month-old WT ($p<0.025$) and Neu3-/- (p=ns) mice spent continuously less time from day one to five, to find the hidden platform (Fig. 7B, D). Our date showed that WT, Hexa-/- and Neu3-/- mice used distal clues more efficiently than Hexa-/-Neu3-/- mice.

Swimming speeds recorded in the Morris water maze were significantly lower at 2.5 and 4.5-month- old Hexa-/-Neu3-/- (7.8 ± 0.8; 8.7 ± 0.6, respectively) mice compared with that in age-matched WT (18.6 ± 1.3, $p < 0.0001$; 16.8 ± 1, $p< 0.0001$, respectively), Hexa-/- (12.7 ± 0.9, $p < 0.0001$; 12 ± 0.9, $p< 0.001$, respectively) and Neu3-/- (10.8 ± 1.2, $p < 0.05$; 20.2 ± 1.3, p = ns, respectively) (Fig. 7E, F). However, the average distance spent to find the target platform was similar in WT, Hexa-/-, Neu3-/- and Hexa-/-Neu3-/- mice in both 2.5 and 4.5-month-old mice groups (Fig. 7G, H).

Typical swim patterns revealed that both 2.5 and 4.5-month-old Hexa-/-Neu3-/- mice were unable to find the escape platform by the final day of the test, whereas age-matched WT, Hexa-/- and Neu3-/- mice were successful at using clues to find it. In addition, 4.5-month-old mice showed more anxiety-related behaviors compared with that in WT and single deficient Hexa-/- and Neu3-/- mice (Fig. 7I, J).

The 5 min open-field test was performed to measure levels of anxiety [49]. A significant difference was detected between WT and Hexa-/-Neu3-/- mice ($p<0.001$ for 2.5 months; $p< 0.025$ for 4.5 months) in age-independent manner. Moreover, Hexa-/-Neu3-/- (291.2 ± 1.8 s for 2.5 months; 288.4 ± 2.1 s for 4.5 months) mice spent most of the time in the periphery of the open field compared to WT (256.3 ± 7.5 s for 2.5 months; 268.3 ± 4.1 s for 4.5 months), Hexa-/- (275.4 ± 3.2 s for 2.5 months; 284.4 ± 3.1 s for 4.5 months) and Neu3-/- (273 ± 7.2 s for 2.5 months; 277.2 ± 3.3 s for 4.5 months). The walking patterns and the amount of time spent in the center and the periphery of the open field area indicated that both, 2.5 and 4.5-month-old Hexa-/-Neu3-/- mice displayed more anxiety-related behaviors, compared to the other genotypes according to the walking patterns and the amount of time spent in the center and the periphery of the open field area (Supp. Fig. 7).

Deficits in cognitive learning and memory

The passive avoidance test was used to detect cognitive learning and memory deficits [47]. We found that 2.5-month-old WT, Hexa-/-, Neu3-/- and Hexa-/-Neu3-/- mice re-entered the dark compartment at the average times: 219 ± 41.3 s, 203 ± 31.8 s, 132 ± 21.8 s, and 118 ± 60 s, respectively, after having previously received the electric shock through the feet. These results may indicate that the younger age group could not tolerate light and prefer the dark compartment despite of the 0.2 mA electric shock, for 2 s (Fig. 8A). Nearly all the 4.5-month-old WT mice avoided entrance into the dark compartment during the 300 s observation period, whereas the Hexa-/-Neu3-/- mice re-entered the chamber at an average time of 160 s (292.1 ± 7.9 s in WT and 159 ± 33.5 s in Hexa-/-Neu3-/-; $p<0.001$). In addition, Hexa-/- and Neu3-/- mice re-entered the chamber in slightly less time than WT mice (Fig. 8B). These results may show that Hexa-/-Neu3-/- mice display a significant deterioration in memory function compared with that in other groups.

Deficits in neuromotor behaviour

In a previous work, Hexa-/-Neu3-/- mice exhibited progressively impaired performance on the rotarod test [5]. This test is used to evaluate motor skill learning and involves endurance, motor coordination and muscle strength [50]. The Morris water maze test showed that both 2.5 and 4.5-month-old Hexa-/-Neu3-/-

mice lost their swimming speed, which could be related with deterioration in motor coordination and muscle strength (Fig. 7E, F). For a more specific measure of muscle strength, grip strength tests were performed [47, 50]. The fore limb assessments demonstrated no significant change in strength of mice at the 2.5 months of age (Fig. 9A). The strength of Hexa-/- and Hexa-/-Neu3-/- mice was significantly impaired compared to WT mice at 4.5 months of age (87 ± 4.7 in WT, 56.2 ± 6.1 in Hexa-/- , 82 ± 11.2 in Neu3-/- and 26.5 ± 10.5 in Hexa-/-Neu3-/-). Overall, Hexa-/-Neu3-/- mice displayed the most dramatic muscle strength impairment and functional deterioration ($p< 0.025$). This result could be related to abnormal GM2 accumulation in the muscles of *Hexa-/-Neu3-/-* mice [5].

Discussion

Neuroinflammation is a common hallmark in the pathogenesis of several lysosomal storage disorders including GM2 gangliosidosis and may negatively impact neuronal survival [17, 20]. In a previous study, we showed that severe astrogliosis and neurodegeneration in the hippocampus, cerebral cortex, and thalamus of Hexa-/-Neu3-/- mice correlated with undegraded GM2 accumulation [5]. However, the mechanism of disease progression relevant to neuroinflammation was not yet elucidated. In the present work, we focused on investigating the molecular, immune, histochemical, behavioral and age-dependent mediators of neuroinflammation in Hexa-/-Neu3-/- mice.

It has been shown that the accumulation of undegraded gangliosides linked to activation of microglial cells [32, 51]. Here, we showed that accumulation of GM2 led to the activation of the microglial/macrophage system in the brain and retina of Hexa-/-Neu3-/- mice compared with that in age-matched WT, Hexa-/- and Neu3-/- mice (Supp. Fig. 1, Fig. 2). Activation of this cellular system led to an altered expression profile of both pro- and anti-inflammatory cytokines and chemokines, in the cortex and cerebellum. We found that while pro-inflammatory cytokines and chemokines, such as Ccl2, Ccl3, Ccl4 and Cxcl10 were significantly up-regulated significantly in the brain of Hexa-/-Neu3-/- compared with that in Hexa-/- mice, anti-inflammatory cytokines and chemokines such as IL10, IL13, IL11 and IL24 were significantly (Fig. 1). It has been shown that simultaneous increase of Ccl2, Ccl3 and Ccl5 in mice brain leads to epileptic seizures [52]. These elevated levels may account for neuroinflammation and the seizure activity observed in the pathology of early-onset Tay-Sachs disease mouse model.

Ccl2, Ccl3 and Cxcl10 play a role in the attraction, migration and activation of monocytes, lymphocytes, and neutrophils in the CNS [19, 25, 26]. Their increased levels in the CNS of Hexa-/-Neu3-/- mice triggered PBMC infiltration similar to the Sandhoff mouse model. This data suggest that inhibition of PBMC infiltration may delay disease progression and neurodegeneration in Hexa-/-Neu3-/- mice similar to the Hexb-/-Ccl2-/- mice [38]. Moreover, it was reported that deletion of Ccl3 gene caused a delay of neuronal loss in Sandhoff mice (Hexb-/-Mip1α-/- mice) by inhibiting macrophage infiltration to the inflammatory sites, which resulted in improved neurologic status and a longer lifespan (Wu and Proia 2004). Additionally, Hexb-/-Tnfα-/- mice resulted in a delayed neurodegenerative cascade by an extending lifespan, improving sensorimotor coordination, decreasing levels of astrogliosis and neuronal cell death

[53]. We suggest that adding antagonists of pro-inflammatory cytokines and chemokines such as Ccl3 or Ccl4 in daily feeding of Hexa-/-Neu3-/- mice may reverse neuroinflammatory conditions.

Activated microglia produces various pro-inflammatory mediators, chemokines and cytokines which negatively impact neurons and oligodendrocytes [42]. Here, we showed that, Hexa-/-Neu3-/- mice exhibited significant loss in neuronal density (Fig. 4) and oligodendrocytes (Fig. 5). These results are consistent with the previous research indicating increased apoptotic cell death in the brain of Hexa-/-Neu3-/- mice. [5]. Furthermore, transcription levels of IL 11, whose over expression has been shown to inhibit demyelinization by protecting oligodendrocytes [54], was significantly reduced in both the cortex and cerebellum of Hexa-/-Neu3-/- mice compared with that in Hexa-/- mice (Fig. 1).

Deficiencies in memory, spatial and cognitive learning in Hexa-/-Neu3-/- mice, demonstrated by Morris water maze and passive avoidance test, might be related to abnormal GM2 accumulation in CNS (Supp. Fig. 1) as well as reduction in neuronal density (Fig. 4) and oligodendrocytes (Fig. 5). Oligodendrocytes are necessary for optimal signal transduction [32, 42]. Additionally, deficits in memory and learning might be related to impaired hippocampus , which is involved in spatial and/or temporal processing of memory [55], deterioration of Purkinje cells, which play a role in spatial navigation [5, 56] and/or damaged retrosplenial and secondary motor cortex, which are involved in memory, navigation, the control of movement [57]. Memory impairments of Hexa-/-Neu3-/- mice, observed in the passive avoidance test, might also be accounted by a decreased sensitivity to electric shock, due to damage in primary motor and somatosensory cortex, which are regions that process pain control [58].

The swimming speeds of 2.5- and 4.5-month-old Hexa-/-Neu3-/- mice were significantly lower than those of age-matched control groups, although they move equal amounts of distance to find the target platform (Fig. 7). These data suggest that Hexa-/-Neu3-/- mice may not be able to learn the location of the hidden platform due to the memory impairment and damaged signaling pathways in the CNS.

Conclusion

In conclusion, our data suggest that abnormal GM2 accumulation in the CNS of early-onset Tay-Sachs disease mouse model activates neuroinflammation by triggering the release of pro-inflammatory cytokines and chemokines, microgliosis, astrogliosis and the infiltration of PBMC in the CNS. This inflammatory cascade results in loss of oligodendrocytes and neurons and consequent behavioral alterations. These observations collectively suggest that modulation of Ccl2, Ccl3 and Cxcl10 or of their receptors, in combination with traditional drugs such as Propagermanium, may provide a novel approach for the management of Tay-Sachs disease.

Abbreviations

IL6R: Interleukin-6 receptor; MBP: Myelin basic protein; TNFα: Tumor necrosis factor-α; TSD: Tay-Sachs disease; SD: Sandhoff disease; KO: Knockout; TNFα: Tumor necrosis factor-α; IL1β: Interleukin 1 beta;

TGFβ1: Transforming growth factor beta 1; IL10: Interleukin 10; IL11: Interleukin 11; IL13: Interleukin 13; IL2: Interleukin 2; IL22: Interleukin 22; IL4: Interleukin 4; ENA-78: Epithelial neutrophil- activating protein 78; TNFR2:Tumor necrosis factor receptor-2; MCP-1/Ccl2: Monocyte Chemoattractant Protein-1/C-C motif chemokine ligand 2; MIP-1α/Ccl3: Macrophage inflammatory protein 1 alpha/C-C motif chemokine ligand 3; MIP-1β/Ccl4: Macrophage ınflammatory protein 1 beta/C-C motif chemokine ligand 4; IP-10 / Cxcl10: Interferon-inducible protein 10/ chemokine interferon-γ inducible protein 10; Bmp2: Bone morphogenetic protein 2 ; Bmp4: Bone morphogenetic protein 4; Bmp6: Bone morphogenetic protein 6; Bmp7: Bone morphogenetic protein 7; Csf3: Colony-stimulating factor 3; Csf1: Colony-stimulating factor 1; Lif: Leukemia Inhibitory Factor; BBB: Blood–brain barrier; PBMC: Peripheral blood mononuclear cell; MAG: Myelin-associated glycoprotein; Gusb: Beta-glucuronidase; Hprt: Hypoxanthine-guanine phosphoribosyltransferase; Hsp90ab1: Heat Shock Protein 90 Alpha Family Class B Member ; GADPH: D-Glyceraldehyde-3-Phosphate Dehydrogenase; Actb: Beta-actin; PCR: Polymerase chain reaction; PBS: Phosphate-buffered saline; OCT: Optimal cutting temperature; BSA: Bovine serum albumin; anti-Moma2: Monocyte and Macrophage antibody; anti-LAMP1: Lysosomal-associated membrane protein 1 antibody; anti-NeuN: Neuronal Marker antibody; anti-CNPase: 2',3'-cyclic nucleotide 3' phosphodiesterase antibody.

Declarations

Acknowledgments

The authors thank Kyowa Hakko Kirin Co., Ltd. (Tokyo, Japan), for a generous gift of monoclonal antibodies against GM2 ganglioside and Dr. Çigdem Tosun (İzmir Institute of Technology, İzmir, Turkey) for the gift of anti-CD45 and anti-IL6 antibody.

Author’s contributions

SAD and VS designed the studies, interpreted the results and wrote the manuscript. The following authors carried out experiments and collected data: SAD, ZKT, NA, LAM. SAD performed anti-GM2, anti-Moma2, anti-CD45, anti-NeuN and anti-CNPase staining, and the behavioral tests with statistical analysis. ZKT performed the determination of cytokines and chemokines with the statistical analysis. NA performed the anti - IL6 staining with statistical analysis. LAM performed the retina analysis.

Funding

Major parts of this study were supported by an EMBO 2010 Installation Grant to Prof Dr. Volkan Seyrantepe.

Availability of data and materials

All data generated or analyzed during this study are included in this published article and its supplementary information files.

Ethics approval and consent to participate

All animal experiments were performed in accordance with the Turkish Institute of Animal Health guide for the care and use of laboratory animals. The animal studies were approved by the Institutional Animal Care and Use Committee of the Izmir Institute of Technology.

Consent for publication

Not applicable.

Competing interests

The authors declare that the research was conducted in the absence of any commercial or financial relationships that could be construed as a potential conflict of interest.

References

1. Yamanaka S, Johnson MD, Grinberg A, Westphal H, Crawley JN, Taniike M, et al. Targeted disruption of the Hexa gene results in mice with biochemical and pathologic features of Tay-Sachs disease. Proc Natl Acad Sci U S A. 1994;91:9975–9.
2. Sango K, Yamanaka S, Hoffmann A, Okuda Y, Grinberg A, Westphal H, et al. Mouse models of Tay–Sachs and Sandhoff diseases differ in neurologic phenotype and ganglioside metabolism. Nat Genet. 1995;11:170–6.
3. Phaneuf D, Wakamatsu N, Huang J, Borowski A, Peterson AC, Fortunato SR, et al. Dramatically different phenotypes in mouse models of human Tay-Sachs and Sandhoff diseases. Hum Mol Genet. 1996;5:1–14.
4. Yuziuk JA, Bertoni C, Beccari T, Orlacchio A, Wu Y-Y, Li S-C, et al. Specificity of Mouse G M2 Activator Protein and β- N -Acetylhexosaminidases A and B. J Biol Chem. 1998;273:66–72.
5. Seyrantepe V, Demir SA, Timur ZK, Von Gerichten J, Marsching C, Erdemli E, et al. Murine Sialidase Neu3 facilitates GM2 degradation and bypass in mouse model of Tay-Sachs disease. Exp Neurol. 2018;299 July 2017:26–41.
6. Jeyakumar M, Thomas R, Eliott-Smith E, Smith DA, Spoel AC Van Der, d'Azzo A, et al. Central nervous system inflammation is a hallmark of pathogenesis in mouse models of GM1 and GM2 gangliosidosis. Brain. 2003;126:974–87.
7. Wada R, Tifft CJ, Proia RL. Microglial activation precedes acute neurodegeneration in Sandhoff disease and is suppressed by bone marrow transplantation. PNAS. 2000;97:10954–9.
8. Myerowitz R. Molecular pathophysiology in Tay-Sachs and Sandhoff diseases as revealed by gene expression profiling. Hum Mol Genet. 2002;11:1343–51.
9. Hayase T, Shimizu J, Goto T, Nozaki Y, Mori M, Takahashi N, et al. Unilaterally and rapidly progressing white matter lesion and elevated cytokines in a patient with Tay – Sachs disease. Brain Dev. 2010;32:244–7.
10. Utz JRJ, Crutcher T, Schneider J, Sorgen P, Whitley CB. Biomarkers of central nervous system inflammation in infantile and juvenile gangliosidoses. Mol Genet Metab. 2015;114:274–80.

11. Baudry M, Yao Y, Simmons D, Liu J, Bi X. Postnatal development of inflammation in a murine model of Niemann-Pick type C disease: Immunohistochemical observations of microglia and astroglia. Exp Neurol. 2003;184:887–903.
12. Farfel-Becker T, Vitner EB, Pressey SNR, Eilam R, Cooper JD, Futerman AH. Spatial and temporal correlation between neuron loss and neuroinflammation in a mouse model of neuronopathic Gaucher disease. Hum Mol Genet. 2011;20:1375–86.
13. Wilkinson FL, Holley RJ, Langford-Smith KJ, Badrinath S, Liao A, Langford-Smith A, et al. Neuropathology in mouse models of mucopolysaccharidosis type I, IIIA and IIIB. PLoS One. 2012;7.
14. Kollmann K, Uusi-Rauva K, Scifo E, Tyynelä J, Jalanko A, Braulke T. Cell biology and function of neuronal ceroid lipofuscinosis-related proteins. Biochim Biophys Acta - Mol Basis Dis. 2013;1832:1866–81.
15. Yamaguchi K, Shiozaki K, Moriya S, Koseki K, Wada T, Tateno H, et al. Reduced susceptibility to colitis-associated colon carcinogenesis in mice lacking plasma membrane-associated sialidase. PLoS One. 2012;7.
16. Calhan OY, Seyrantepe V. Mice with Catalytically Inactive Cathepsin A Display Neurobehavioral Alterations. Behav Neurol. 2017;2017 January.
17. Vitner EB, Platt FM, Futerman AH. Common and uncommon pathogenic cascades in lysosomal storage diseases. J Biol Chem. 2010;285:20423–7.
18. Zhang J-M, An J. Cytokines, Inflammation, and Pain. Int Anesthesiol Clin. 2007;45:27–37.
19. Reichel CA, Rehberg M, Lerchenberger M, Berberich N, Bihari P, Khandoga AG, et al. Ccl2 and Ccl3 mediate neutrophil recruitment via induction of protein synthesis and generation of lipid mediators. Arterioscler Thromb Vasc Biol. 2009;29:1787–93.
20. Bosch ME, Kielian T. Neuroinflammatory paradigms in lysosomal storage diseases. Front Neurosci. 2015;9 OCT:1–11.
21. Arfi A, Richard M, Gandolphe C, Bonnefont-Rousselot D, Thérond P, Scherman D. Neuroinflammatory and oxidative stress phenomena in MPS IIIA mouse model: The positive effect of long-term aspirin treatment. Mol Genet Metab. 2011;103:18–25.
22. Villani lielmo RD, Gargiulo N, Faraonio R, Castaldo S, Reyero EG y, Natale P Di. Cytokines, neurotrophins, and oxidative stress in brain disease from mucopolysaccharidosis IIIB. J Neurosci Res. 2007;85:612–22.
23. Vitner EB, Farfel-Becker T, Eilam R, Biton I, Futerman AH. Contribution of brain inflammation to neuronal cell death in neuronopathic forms of Gaucher's disease. Brain. 2012;135:1724–35.
24. Pandey MK, Jabre NA, Xu YH, Zhang W, Setchell KDR, Grabowski GA. Gaucher disease: Chemotactic factors and immunological cell invasion in a mouse model. Mol Genet Metab. 2014;111:163–71.
25. Mirones I, De Prada I, Gómez AM, Luque A, Martín R, Pérez-Jiménez MÁ, et al. A role for the CXCR3/CXCL10 axis in rasmussen encephalitis. Pediatr Neurol. 2013;49:451–7.

26. Zhang X, Shen J, Man K, Chu ESH, Yau TO, Sung JCY, et al. CXCL10 plays a key role as an inflammatory mediator and a non-invasive biomarker of non-alcoholic steatohepatitis. J Hepatol. 2014;61:1365–75.
27. Shah N, Kammermeier J, Elawad M, Glocker EO. Interleukin-10 and interleukin-10-receptor defects in inflammatory bowel disease. Curr Allergy Asthma Rep. 2012;12:373–9.
28. Bach JP, Rinn B, Meyer B, Dodel R, Bacher M. Role of MIF in inflammation and tumorigenesis. Oncology. 2008;75:127–33.
29. Pastore N, Brady OA, Diab HI, Martina JA, Sun L, Huynh T, et al. TFEB and TFE3 cooperate in the regulation of the innate immune response in activated macrophages. Autophagy. 2016;12:1240–58.
30. Sykaras N, Opperman LA. Bone morphogenetic proteins (BMPs): how do they function and what can they offer the clinician? J Oral Sci. 2003;45:57–73.
31. Yue X, Wu L, Hu W. The regulation of leukemia inhibitory factor. Cancer cell Microenviron. 2015;2:e877.
32. Rasband MN. Glial Contributions to Neural Function and Disease. Mol Cell Proteomics. 2016;15:355–61.
33. Ohmi K, Greenberg DS, Rajavel KS, Ryazantsev S, Li HH, Neufeld EF. Activated microglia in cortex of mouse models of mucopolysaccharidoses I and IIIB. Proc Natl Acad Sci. 2003;100:1902–7. 34. Chen KH, Chien Y, Wang KL, Leu HB, Hsiao CY, Lai YH, et al. Evaluation of Proinflammatory Prognostic Biomarkers for Fabry Cardiomyopathy With Enzyme Replacement Therapy. Can J Cardiol. 2016;32:1221.e1-1221.e9.
34. Donida B, Marchetti DP, Biancini GB, Deon M, Manini PR, da Rosa HT, et al. Oxidative stress and inflammation in mucopolysaccharidosis type IVA patients treated with enzyme replacement therapy. Biochim Biophys Acta - Mol Basis Dis. 2015;1852:1012–9.
35. Kitatani K, Wada M, Perry D, Usui T, Sun Y, Obeid LM, et al. Activation of p38 mitogen-activated protein kinase in Gaucher's disease. PLoS One. 2015;10:1–9.
36. da Fonseca ACC, Matias D, Garcia C, Amaral R, Geraldo LH, Freitas C, et al. The impact of microglial activation on blood-brain barrier in brain diseases. Front Cell Neurosci. 2014;8 November:1–13.
37. Kyrkanides S, Miller AW, Miller JH, Tallents RH, Sabine M, Olschowka ME, et al. Peripheral blood mononuclear cell infiltration and neuroinflammation in the HexB-/- mouse model of neurodegeneration. J Neuroimmunol. 2009;203:50–7.
38. López-Expósito I. The Impact of Food Bioactives on Health: In Vitro and Ex Vivo Models. SpingerOpen; 2015.
39. Gusel'nikova V V., Korzhevskiy DE. NeuN as a neuronal nuclear antigen and neuron differentiation marker. Acta Naturae. 2015;7:42–7.
40. Keilani S, Lun Y, Stevens AC, Williams HN, Sjoberg ER, Khanna R, et al. Lysosomal Dysfunction in a Mouse Model of Sandhoff Disease Leads to Accumulation of Ganglioside-Bound Amyloid- □ Peptide. J Neurosci. 2012;32:5223–36.

41. Peferoen L, Kipp M, van der Valk P, van Noort JM, Amor S. Oligodendrocyte-microglia cross-talk in the central nervous system. Immunology. 2014;141:302–13.
42. Jackman N, Ishii A, Bansal R. Myelin biogenesis and oligodendrocyte development: parsing out the role of glycosphingolipids. Physiol. 2009;:290–7.
43. Vecino E, Rodriguez FD, Ruzafa N, Pereiro X, Sharma SC. Glia-neuron interactions in the mammalian retina. Prog Retin Eye Res. 2016;51:1–40.
44. Fu H, Cataldi MP, Ware TA, Zaraspe K, Meadows AS, Murrey DA, et al. Functional correction of neurological and somatic disorders at later stages of disease in MPS IIIA mice by systemic scAAV9-hSGSH gene delivery. Mol Ther - Methods Clin Dev. 2016;3 October 2015:16036.
45. Hofmann L, Karl F, Sommer C, Üçeyler N. Affective and cognitive behavior in the alpha-galactosidase A deficient mouse model of Fabry disease. PLoS One. 2017;12:1–14.
46. D'Hooge R, Lüllmann-Rauch R, Beckers T, Balschun D, Schwake M, Reiss K, et al. Neurocognitive and Psychotiform Behavioral Alterations and Enhanced Hippocampal Long-Term Potentiation in Transgenic Mice Displaying Neuropathological Features of Human a-Mannosidosis. J Neurosci. 2005;25:6539–49.
47. Schlegel V, Thieme M, Holzmann C, Witt M, Grittner U, Rolfs A, et al. Pharmacologic treatment assigned for Niemann Pick Type C1 disease partly changes behavioral traits in wild-type mice. Int J Mol Sci. 2016;17:1–17.
48. Seyrantepe V, Lema P, Caqueret A, Dridi L, Hadj SB, Boucher F, et al. Mice Doubly-Deficient in Lysosomal Hexosaminidase A and Neuraminidase 4 Show Epileptic Crises and Rapid Neuronal Loss. PLoS Genet. 2010;6.
49. Foley JW, Bercury SD, Finn P, Cheng SH, Scheule RK, Ziegler RJ. Evaluation of systemic follistatin as an adjuvant to stimulate muscle repair and improve motor function in Pompe mice. Mol Ther. 2010;18:1584–91.
50. Vitner EB, Platt FM, Futerman AH. Common and uncommon pathogenic cascades in lysosomal storage diseases. J Biol Chem. 2010;285:20423–7.
51. Arisi GM, Foresti ML, Katki K, Shapiro LA. Increased CCL2, CCL3, CCL5, and IL-1β cytokine concentration in piriform cortex, hippocampus, and neocortex after pilocarpine-induced seizures. J Neuroinflammation. 2015;12:129.
52. Abo-ouf H, Hooper AWM, White EJ, Rensburg HJJ Van, Trigatti BL, Igdoura SA. Deletion of tumor necrosis factor- a ameliorates neurodegeneration in Sandhoff disease mice. Hum Mol Genet. 2013;22:3960–75.
53. Maheshwari A, Janssens K, Bogie J, Van Den Haute C, Struys T, Lambrichts I, et al. Local overexpression of interleukin-11 in the central nervous system limits demyelination and enhances remyelination. Mediators Inflamm. 2013;2013.
54. Eichenbaum H. On the Integration of Space, Time, and Memory. Neuron. 2017;95:1007–18.
55. Lee J-M, Kim C-J, Park J-M, Song MK, Kim Y-J. Effect of treadmill exercise on spatial navigation impairment associated with cerebellar Purkinje cell loss following chronic cerebral hypoperfusion.

Mol Med Rep. 2018;17:8121–8.

56. Yamawaki N, Radulovic J, Shepherd GMG. A Corticocortical Circuit Directly Links Retrosplenial Cortex to M2 in the Mouse. J Neurosci. 2016;36:9365–74.

57. Lee S, Hwang E, Lee D, Choi JH. Pulse-train Stimulation of Primary Somatosensory Cortex Blocks Pain Perception in Tail Clip Test. Exp Neurobiol. 2017;26:90–6.

Figures

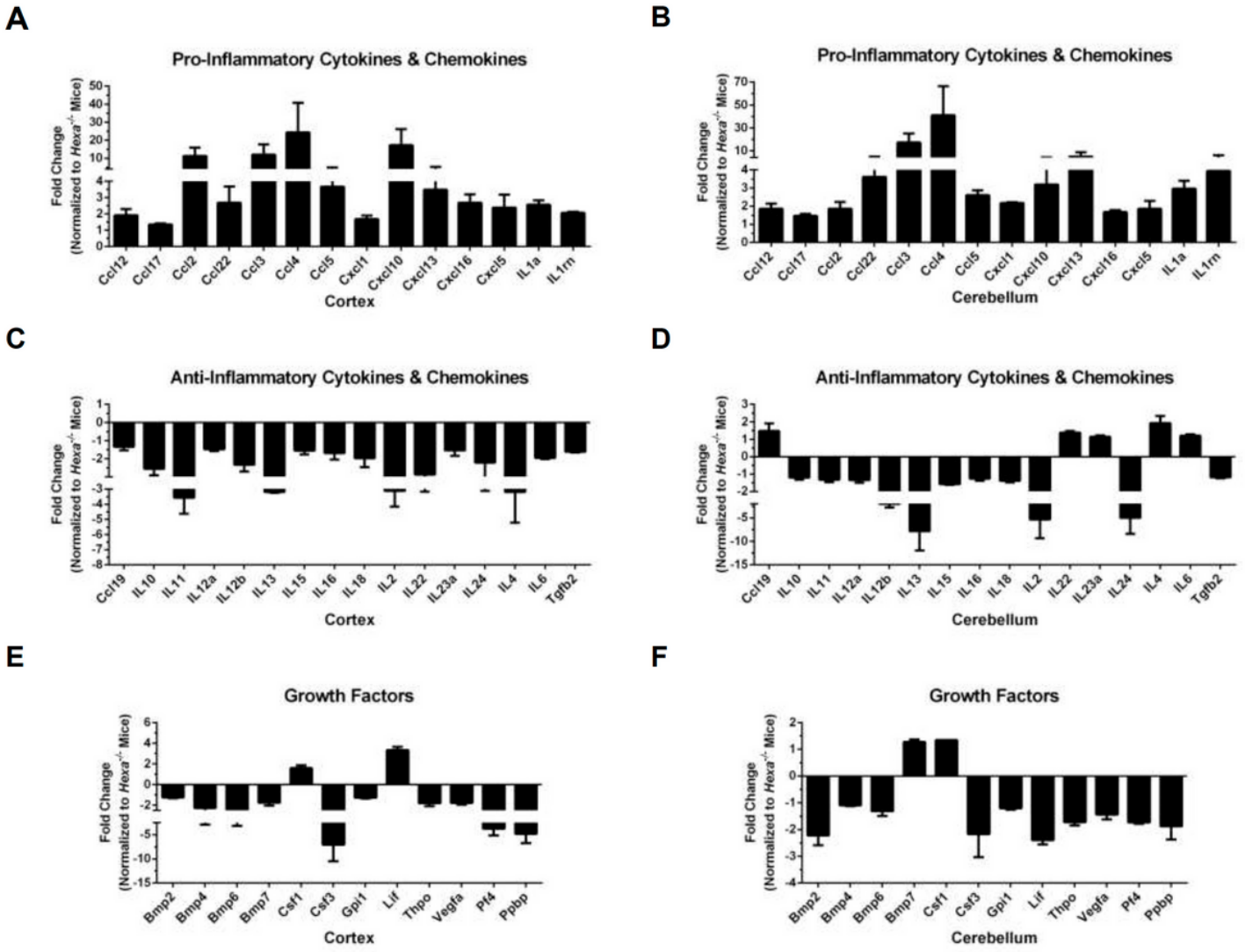

Figure 1

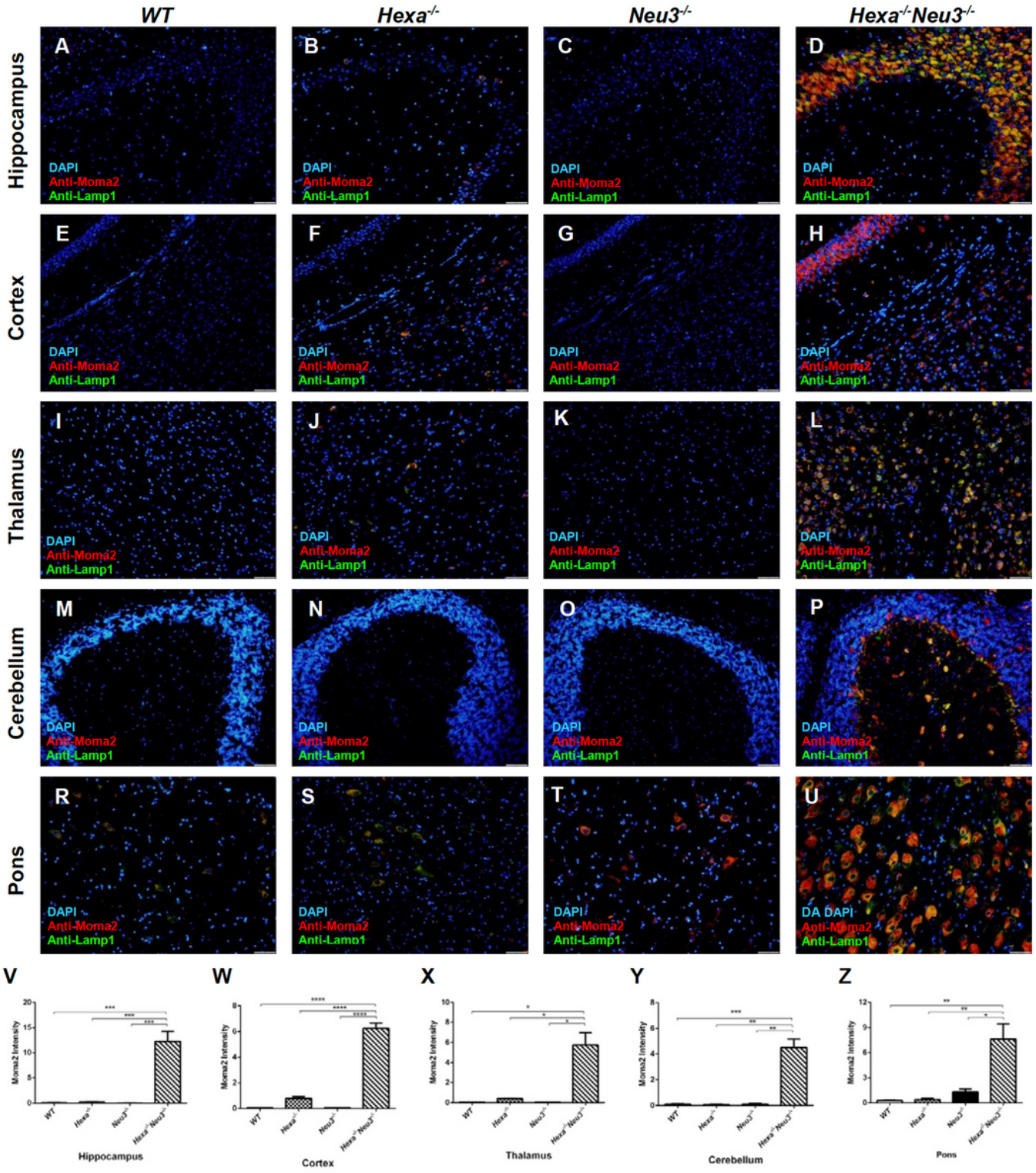
WT
Hexa-/-
Neu3-/-
Hexa-/-Neu3-/-
Hippocampus
Cortex
Thalamus
Cerebellum
Pons
DAPI
Anti-Moma2
Anti-Lamp1
Moma2 Intensity
Hippocampus
Cortex
Thalamus
Cerebellum
Pons

Figure 2

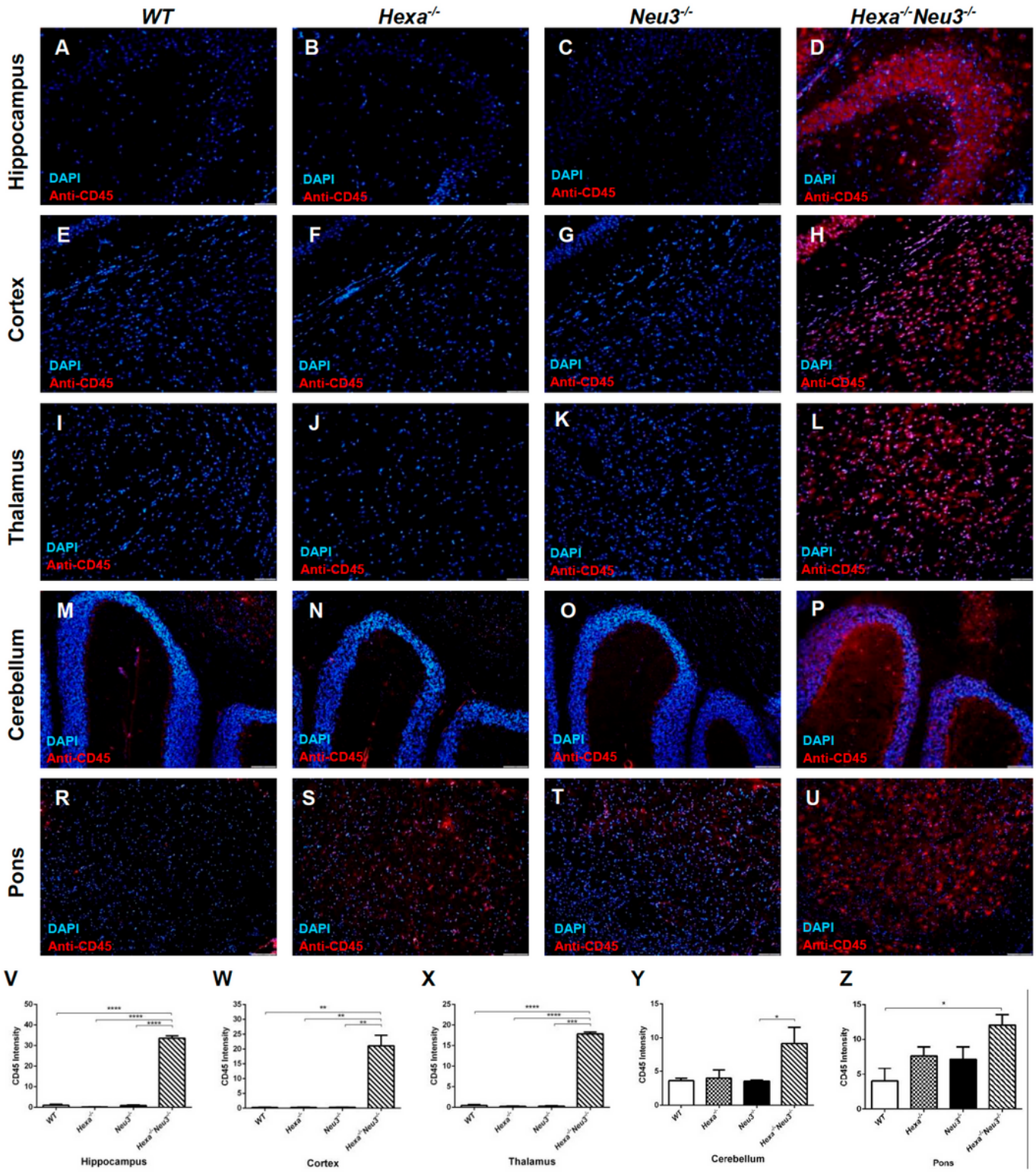
WT
Hexa-/-
Neu3-/-
Hexa-/-Neu3-/-
Hippocampus
Cortex
Thalamus
Cerebellum
Pons
DAPI
Anti-CD45
CD45 Intensity
Hippocampus
Cortex
Thalamus
Cerebellum
Pons

Figure 3

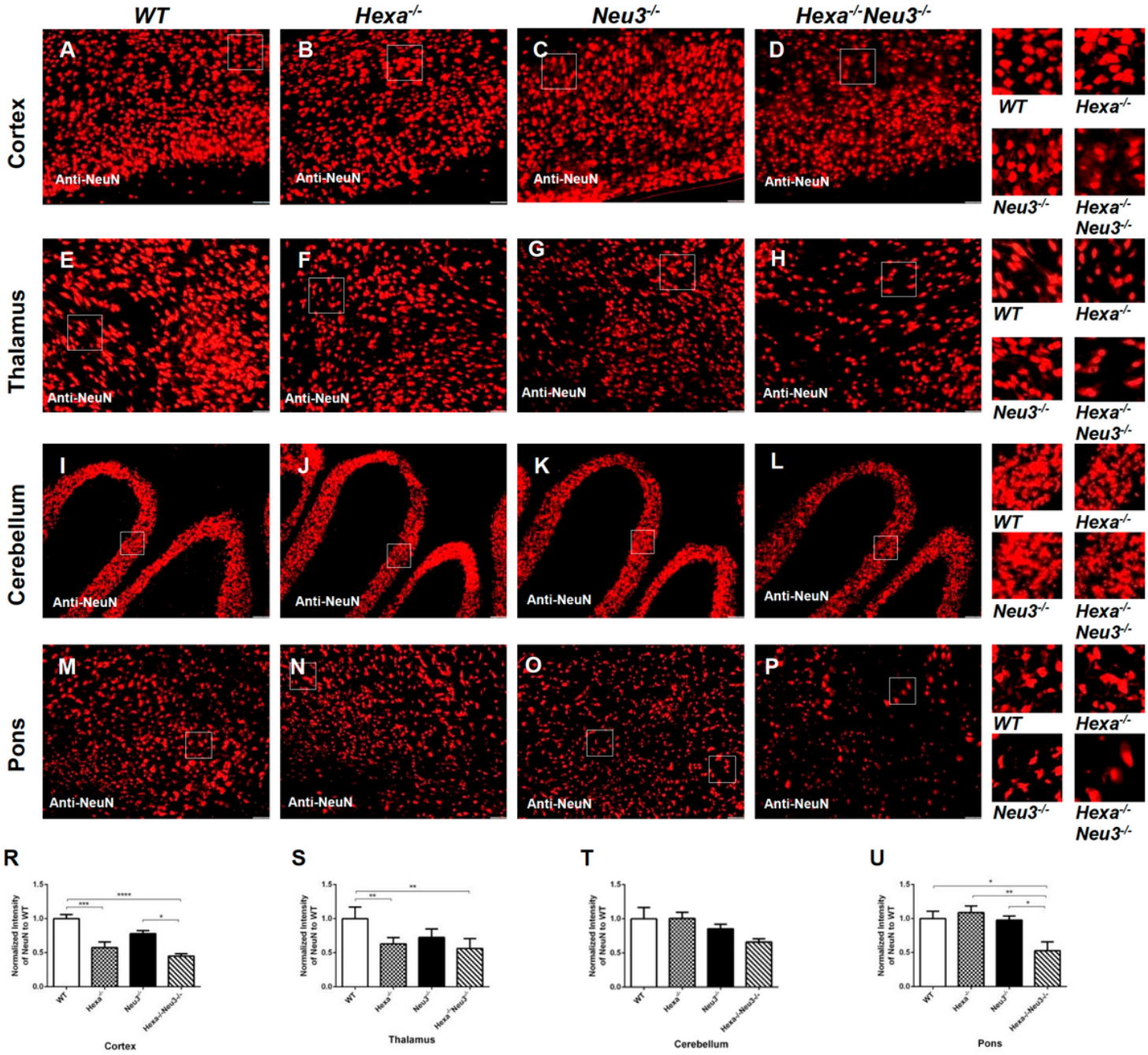
WT
Hexa-/-
Neu3-/-
Hexa-/-Neu3-/-
Cortex
Thalamus
Cerebellum
Pons
A
B
C
D
E
F
G
H
I
J
K
L
M
N
O
P
Anti-NeuN
WT
Hexa-/-
Neu3-/-
Hexa-/- Neu3-/-
R
S
T
U
Normalized Intensity of NeuN to WT
Cortex
Thalamus
Cerebellum
Pons

Figure 4

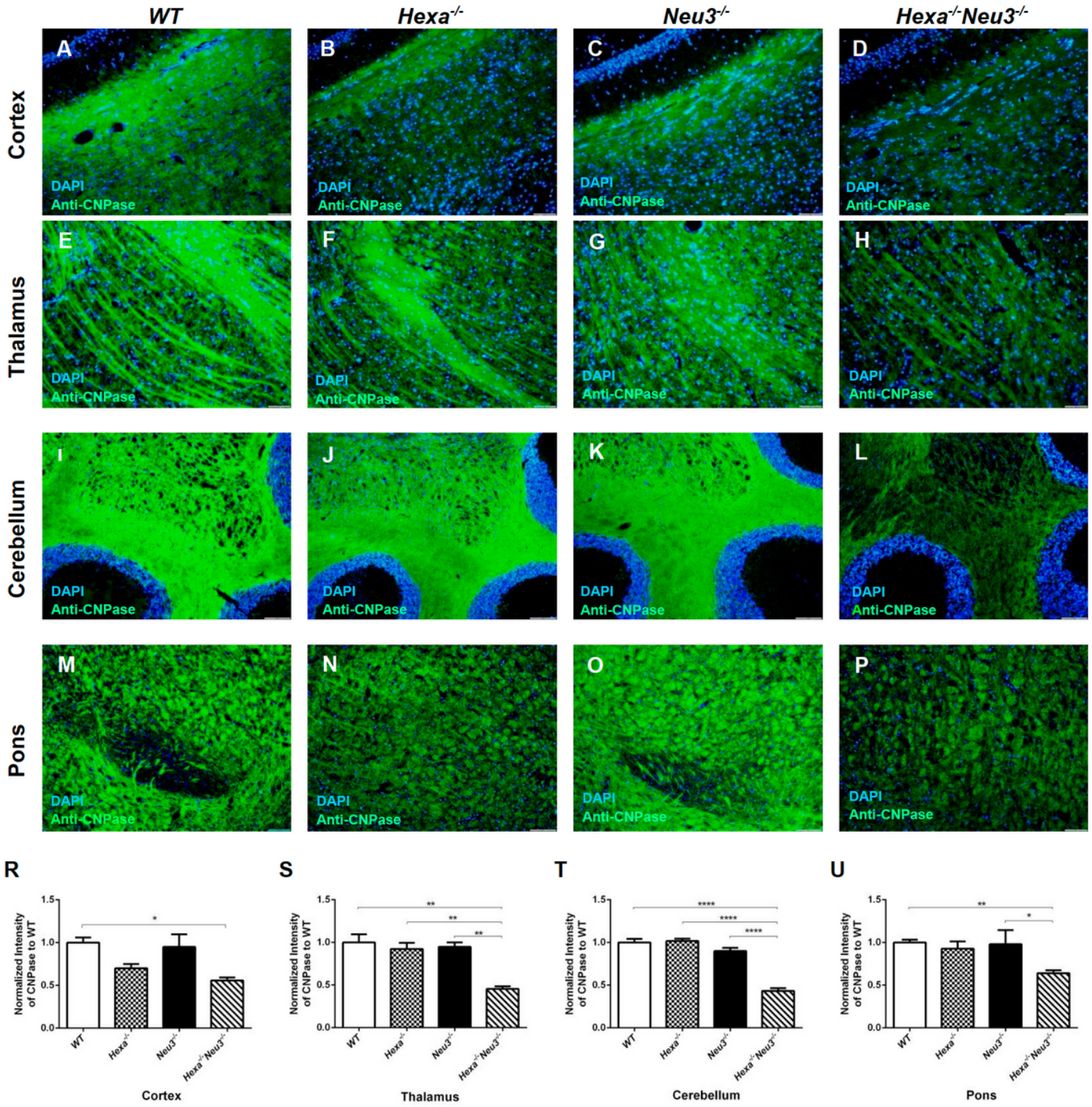
WT
Hexa-/-
Neu3-/-
Hexa-/-Neu3-/-
Cortex
Thalamus
Cerebellum
Pons
A
B
C
D
E
F
G
H
I
J
K
L
M
N
O
P
DAPI
Anti-CNPase
R
S
T
U
Normalized Intensity of CNPase to WT
1.5
1.0
0.5
0.0
WT
Hexa-/-
Neu3-/-
Hexa-/-Neu3-/-
Cortex
Thalamus
Cerebellum
Pons

Figure 5

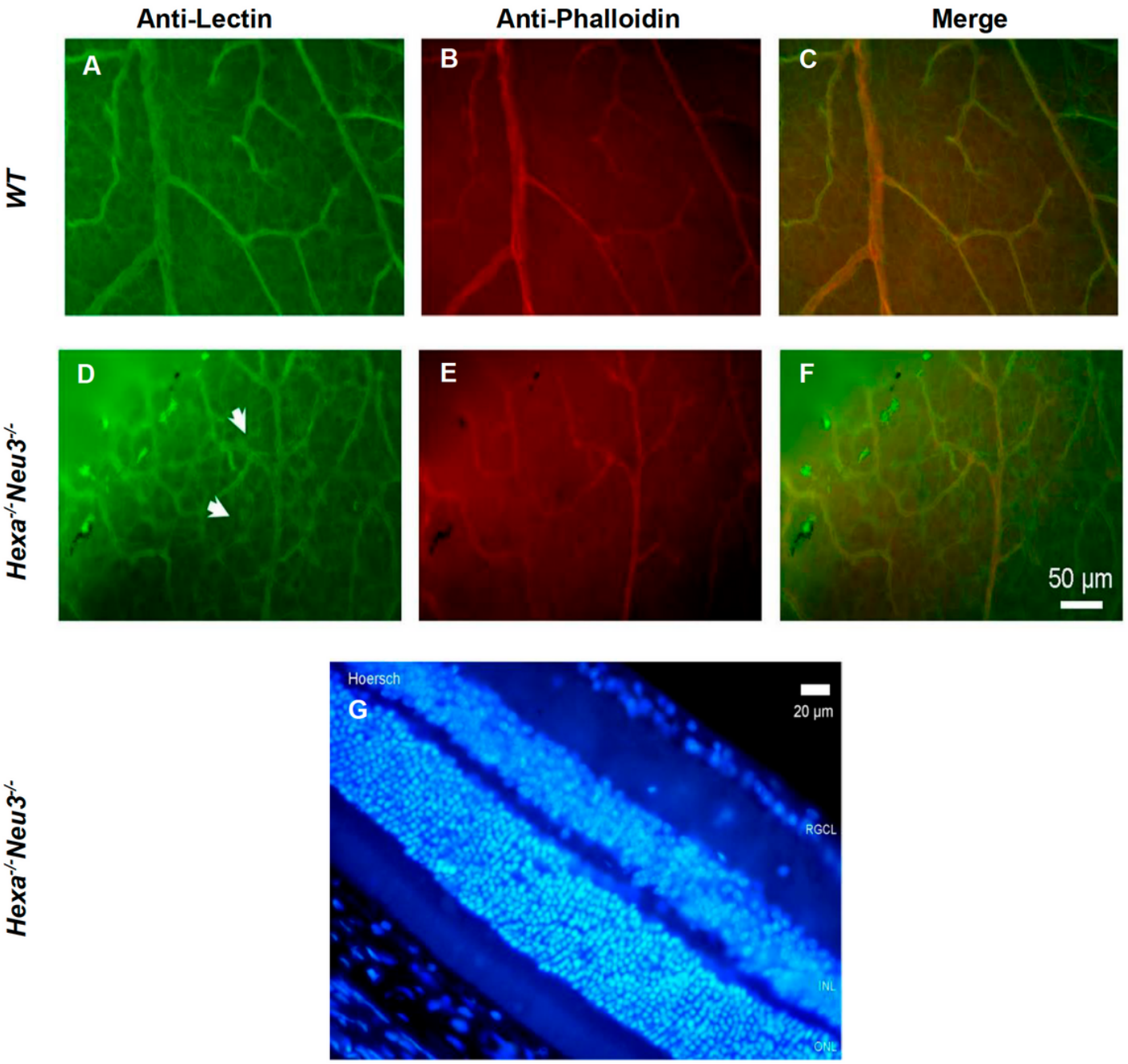
Anti-Lectin
Anti-Phalloidin
Merge
A
B
C
WT
D
E
F
50 µm
Hexa-/-Neu3-/-
Hoersch
G
20 µm
RGCL
INL
ONL
Hexa-/-Neu3-/-

Figure 6

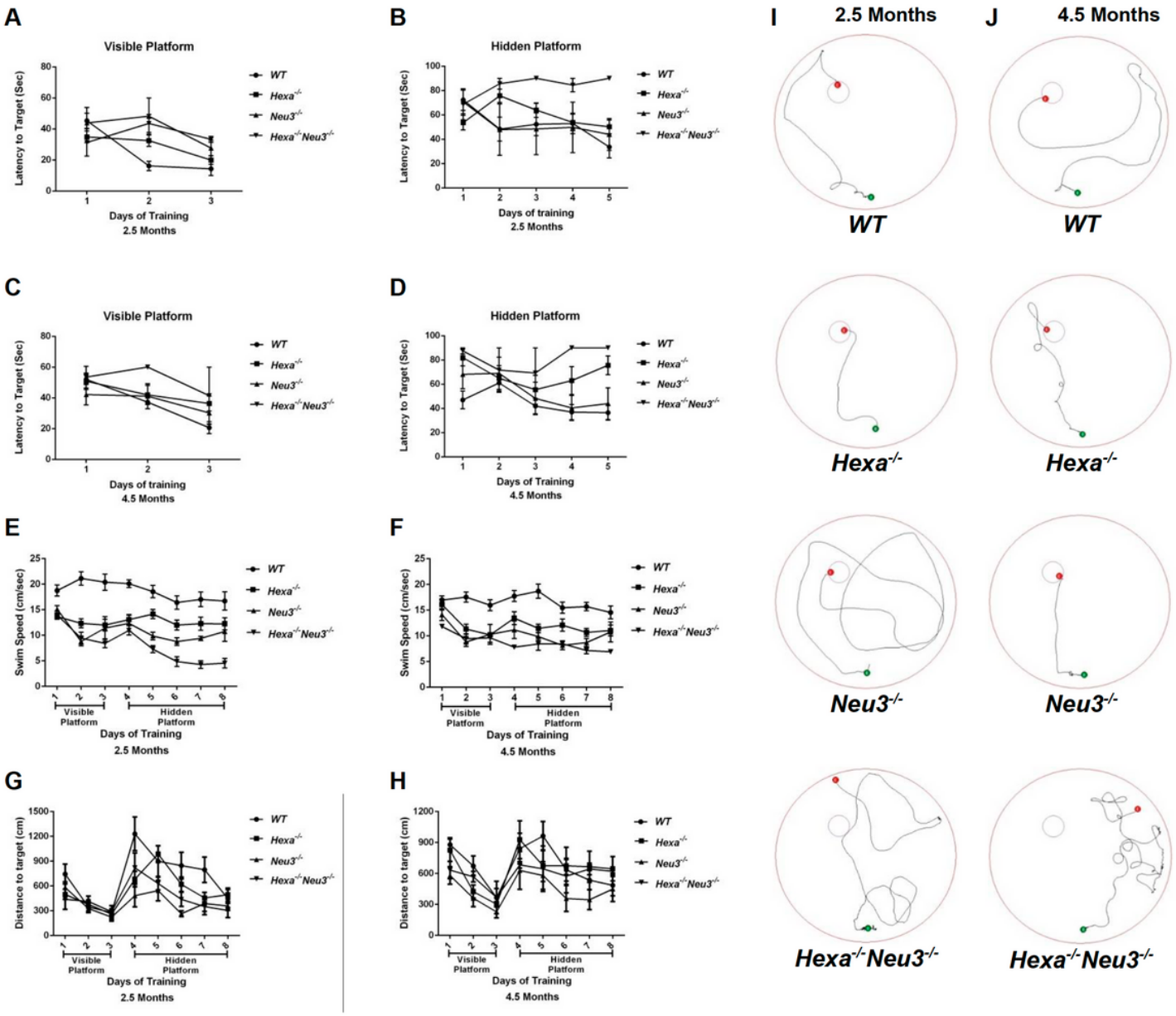
A
Visible Platform
Latency to Target (Sec)
Days of Training
2.5 Months
B
Hidden Platform
Latency to Target (Sec)
Days of training
2.5 Months
I
2.5 Months
J
4.5 Months
WT
Hexa-/-
Neu3-/-
Hexa-/-Neu3-/-
C
Visible Platform
Latency to Target (Sec)
Days of training
4.5 Months
D
Hidden Platform
Latency to Target (Sec)
Days of Training
4.5 Months
Hexa-/-
E
Swim Speed (cm/sec)
Visible Platform
Hidden Platform
Days of Training
2.5 Months
F
Swim Speed (cm/sec)
Visible Platform
Hidden Platform
Days of Training
4.5 Months
Neu3-/-
G
Distance to target (cm)
Visible Platform
Hidden Platform
Days of Training
2.5 Months
H
Distance to target (cm)
Visible Platform
Hidden Platform
Days of Training
4.5 Months
Hexa-/-Neu3-/-

Figure 7

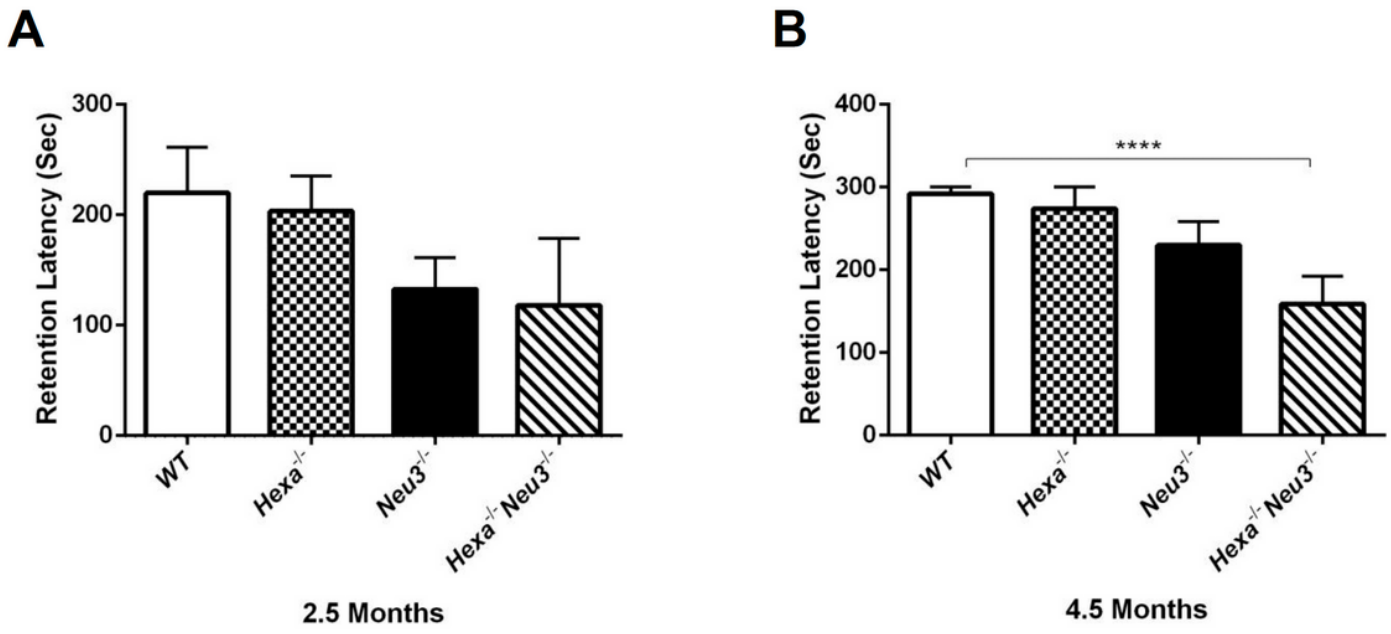

Figure 8

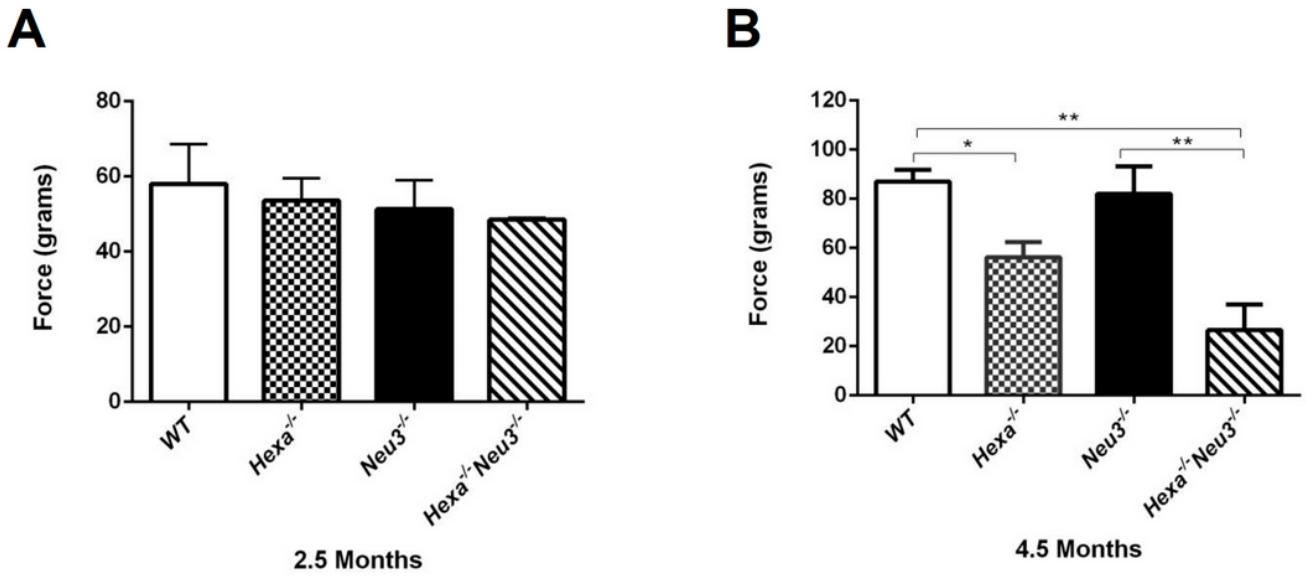

Figure 9

Supplementary Files

This is a list of supplementary files associated with this preprint. Click to download.

- SuppFig2.pdf
- SuppFig4.pdf

- SuppFig1.pdf
- SuppFig6.pdf
- SuppFig5.pdf
- SuppFig7.pdf
- SuppFig3.pdf